LINC00961 Attenuates TGF-β-induced Endothelial-mesenchymal Transition and Myocardial Fibrosis Following Myocardial Infarction

Jinxing Hu
First Affiliated Hospital of Nanchang University
Zeqi Zheng
First Affiliated Hospital of Nanchang University
Ting Kang
First Affiliated Hospital of Nanchang University
Wei Qian
First Affiliated Hospital of Nanchang University
Shanhua Huang
First Affiliated Hospital of Nanchang University
B Li (libingong08@163.com)
Qingdao Municipal Hospital Group https://orcid.org/0000-0002-8363-5276

Research Article

Keywords: LINC00961, TGF-β, myocardial infarction, myocardial fibrosis, endothelial-mesenchymal transition

Posted Date: October 20th, 2021

DOI: https://doi.org/10.21203/rs.3.rs-990440/v1

Abstract

Background

LINC00961 has been implicated in the development of cardiovascular diseases, and its potential mechanisms of action have been suggested. Here, we investigated the role of LINC00961 in the endothelial-mesenchymal transition (EndMT) induced by TGF-β and myocardial fibrosis following myocardial infarction(MI).

Methods and Results

Human cardiac microvascular endothelial cells (HCMECs) and male wild-type (WT) mice were used. HCMECs were exposed to TGF-β in serum-free medium for 48 h to induce EndMT. CCK8 and Flow cytometry analysis were used to examine cell viability and assess apoptosis. To identify $CD31^+/\alpha\text{-}SMA^+$ double-positive cells, immunofluorescence staining was used. Western blotting and PCR were used for protein and mRNA analyses. TGF-β time-dependently contributed to EndMT and injuries of HCMECs, LINC00961 attenuated the injury and EndMT caused by TGF-β. WT and LINC00961 knockout C57BL/6 mice were subjected to left anterior descending coronary artery ligation to trigger MI. Myocardial fibrosis was assessed using H&E and Masson's trichrome staining, and Echocardiography was performed to evaluate cardiac function. Western blotting and PCR were used for protein and mRNA expression analyses. MI contributed to myocardial fibrosis and the reduction of cardiac function, LINC00961 and SB-431542 (TGF-β selective inhibitor) attenuated the reduced cardiac function and myocardial fibrosis following MI.

Conclusion

LINC00961 attenuates EndMT induced by TGF-β and myocardial fibrosis following MI, owing by suppressing the TGF-β pathway, reducing p-SMAD2/3 expression, and inhibiting SNAIL and SLUG.

Introduction

Myocardial infarction (MI) is one of the most prevailing lethal diseases around the world, characterized by inadequate cardiac blood supply, typically developing into myocardial fibrosis[1-3]. MI triggers mass death of cardiomyocyte through necrosis or apoptosis, leading to the reduction of cardiomyocyte number [4, 5]. Although survival following MI has increased with the improvement in medical interventions, cardiac function deterioration cannot be effectively prevented[6, 7]. In the recent past, an incremental number of studies on the regulatory mechanism of myocardial fibrosis following MI confirmed myocardial fibrosis as vital in MI progression [8, 9].

Recently, using qPCR detection, Matsumoto et al. reported a high expression of LINC00961 in human and mouse lung, heart, skeletal muscle, and other tissues [10]. LINC00961, as a newfound long non-coding RNA (lncRNA), encodes a small regulatory polypeptide of amino acid response (SPAAR), displays high

expression levels in heart tissue, and negatively regulates mTORC1 activation[11]. Researchers have begun to study the effects of LINC00961 on cardiovascular diseases[12-15]. For example, Spencer et al. discovered that the LINC00961 transcript and its encoded SPAAR regulate endothelial cell function[16], and Liu et al. demonstrated that LINC00961, via the PI3K/AKT/GSK3β signaling pathway, regulates myocardial infarction [17].

Markwald et al.[18] first discovered Endothelial-mesenchymal transition (EndMT) through heart formation developmental studies in 1975. EndMT is characterized by the decrease of cell–cell adhesion and variations in cell polarity, followed by the induction of a spindle-shaped morphology. These variations mainly refer to reduced endothelial marker expression vascular endothelial cadherin (VE-cadherin) and platelet endothelial cell adhesion molecule-1 (PECAM-1/CD31), and increased mesenchymal marker expression fibroblast specific protein 1 (FSP-1)) and alpha-smooth muscle actin (α-SMA)[19, 20]. Rcently, more and more evidences have manifested that EndMT plays a crucial part in the course of infarction, ischemia-reperfusion, diabetic cardiomyopathy, and myocardial fibrosis[21-24]. Our previous studies have indicated that EndMT can be induced by hypoxia and attenuated by activating AMPK and suppressing mTOR signaling pathway in HCMECs [25-27].

As a secreted cytokine, Transforming growth factor β (TGF-β) can regulate migration, proliferation, and differentiation of different cell types [28]. In addition to the above functions, TGF-β also plays a crucial part in inflammation, tissue repair, and maintaining adult tissue homeostasis, as well as controlling embryogenic development [29]. TGF-β, a member of the TGF-β family, is comprised of TGF-βs, activins, Nodal, bone morphogenetic proteins (BMPs), and so on[30]. All members of the TGF-β family transduce their signals via two types of transmembrane receptors[31]. Nodal, ligand binding of activin, and TGF-β to a constitutively active type II receptor kinase leads to phosphorylation of the type I receptors (activin receptor-like kinase (ALK)-5, ALK-7, and ALK-4), which stimulate signal transduction cascades of downstream in turn, such as receptor-regulated Smad (R-Smad) signaling pathways[30, 31]. Numerous studies have confirmed that TGF-β activates EndMT via the Smad2/3 signaling pathway, and then increasing the expression of cell-adhesion-suppressing transcription factors (TFs), including Slug, Snail, and Twist[29, 32]. SB-431542 (SB), a TGF-β inhibitor, was shown to completely block TGF-β-induced EndMT [33, 34].

Tremendous progress has been made in studying the functions of LINC00961. Nevertheless, whether LINC00961 has a suppressive function on myocardial fibrosis and EndMT has not been elucidated. Here, we have an assumption that LINC00961 suppresses EndMT and myocardial fibrosis following MI by inhibiting the TGF-β-SMAD2/3 signaling pathway.

Materials And Methods

Cell culture, drug treatment, and cell transfection

HCMECs were obtained from ScienCell Research Laboratories (Carlsbad, CA, USA) and cultured in 25-cm^2 cell culture flasks (Corning Inc., Corning, NY, USA) and 5% CO_2 atmosphere at 37 °C. Culture medium was Roswell Park Memorial Institute 1640 (RPMI-1640; Gibco, Grand Island, NY, USA), with 10% fetal bovine serum (FBS; Gibco) and 1% streptomycin / penicillin (Hyclone Laboratories Inc., Logan, UT, USA). HCMECs between passages 4 and 10 were used for the following experiment.

HCMECs were inoculated into six-well plates at a 1 × 10^5 cells/well density in the logarithmic growth phase. Lentiviruses (LV) carrying negative control scrambled RNA and small interfering RNA were applied for transfection in the light of the optimal MOI value. Cells were then exposed to TGF-β1 (10 ng/mL; Peprotech Inc., Rocky Hill, NJ, USA) in serum-free medium[35] for 24, 48, 72, and 96 h, to induce EndMT. Subsequently, the cells were randomly divided into control, TGF-β, TGF-β + LV-control, TGF-β + LV-LINC00961, TGF-β + LV-Sh-control, TGF-β + LV-Sh LINC00961, and LV-Sh LINC0096 + TGF-β + SB431542 groups. SB431542 is a selective inhibitor of TGF-β, was obtained from GlaxoSmithKline Pharmaceuticals (King of Prussia, PA), and dissolved in 100% DMSO (Gibco) at a stock concentration of 10 mmol/L[36]. Following treatment, we collected HCMECs of each group for experimental detection.

Cell Counting Kit 8 (CCK8) assay

HCMECs were seeded into 96-well plates at a 1 × 10^4 cells/well concentration after treatment and transfection. 10 μL CCK8 solution (Beyotime Biotechnology, Shanghai, China) was added to each well, then incubation of 2 h at 37 °C. The absorbance at 450 nm was measured using a microplate reader (Thermo Fisher Scientific, Waltham, MA, USA).

Flow cytometry

We used an annexin V-FITC apoptosis detection kit (Sungene Biotech, Tianjin, China) to monitor the cell apoptosis rate . After treatment and transfection, HCMECs were plated in six-well plates at a 1 × 10^5 cells/well concentration. When 85% confluence was reached, HCMECs were trypsinized and resuspended in 300 μL binding buffer with 5 μL annexin V-FITC. HCMECs were stained with 5 μL propidium iodide (PI) after 10 min of incubation at room temperature in the dark. Eventually, the HCMECs of each group were analyzed using a BD FACS AriaIII flow cytometer with FACSDiva software v 8.0.3 (BD Biosciences, Franklin Lakes, NJ, USA).

Immunofluorescence staining

After fixed with 4% paraformaldehyde for about 20 min, HCMECs were permeabilized in phosphate-buffered saline (PBS) with 0.1% Triton-X100 for 10 min. Then, HCMECs were blocked for 1 h with 5% bovine serum albumin (BSA) and incubated overnight at 4 ℃ with primary antibody α-SMA (14395-1-AP, 1:5,000; ProteinTech Group, Chicago, IL, USA) and CD31 (Sc-376764, 1:500; Santa Cruz Biotechnology Inc., Dallas, TX, USA). Finally, HCMECs were incubated for 1 h with appropriate secondary antibodies (HRP-goat anti-rabbit, AS1107, 1:10,000; ASPEN, Wuhan, China) at room temperature. We used

fluorescence microscopy (Olympus BX51; Olympus, Corporation, Tokyo, Japan) to visualize immunofluorescence.

Animal models

Animal experiment were approved by the Laboratory Animal Ethics Committee of the First Affiliated Hospital of Nanchang University. Wild-type (WT) mice (C57BL/6) were purchased from Guangzhou Jennio Biotech Co., Ltd., (Guangzhou, China), and we created a LINC00961 knockout ($LINC00961^{-/-}$) mouse model using CRISPR/Cas-mediated genome engineering. All mice were bred at the Jiangxi Institute of Hypertension (Nanchang, China). 8-wk-old WT and $LINC00961^{-/-}$ male mice were subjected to left anterior descending (LAD) coronary artery permanent ligation using a 7-0 silk suture to induce MI, as previously described. Except the LAD was not ligated, the sham procedure was identical. We randomly divided the mice into $LINC00961^{-/-}$ + Sham, WT + Sham, $LINC00961^{-/-}$ + MI, and WT + MI, $LINC00961^{-/-}$ + MI + SB, and WT + MI + SB groups (n = 5).

Cardiac function

After anesthetized with 3% pentobarbital sodium at a 40 mg/kg dose by intraperitoneal injection, the mice were fixed in the supine position. The cardiac function of mice was measured using the Vevo 770 imaging system with an ACUSON X150 ultrasound system (Siemens, Munich, Germany). The echocardiographic parameters included M-mode ultrasound images of the parasternal left long-axis section, left ventricular fractional shortening (LVFS), left ventricular end-diastolic diameter (LVEDD), left ventricular ejection fraction (LVEF), and left ventricular end-systolic diameter (LVESD).

Histological analysis

Tissues were fixed in 4% paraformaldehyde, sectioned, then processed for hematoxylin-eosin and Masson's trichrome immunohistochemical staining. The antibodies used for immunohistochemical analysis were anti-mouse CD31 (Sc-376764, 1:500; Santa Cruz Biotechnology), α-SMA (14395-1-AP, 1:5,000; ProteinTech Group), VE-cadherin (36-1900, 1:500; Thermo Fisher Scientific, Waltham, MA, USA), and FSP-1 (20886-1-A, 1:1,000; ProteinTech Group, Chicago, IL, USA).

Quantitative real-time PCR

We used TRIpure Extraction Reagent (ELK Biotechnology, Wuhan, China) to isolate total RNA from HCMECs and mice hearts. Synthesis of cDNA: heating the reactant to 85 °C for 5 min, followed by 40 cycles of 85 °C for 10 s, 60 °C for 30 s, and 70 °C for 30 s. Real-time quantitative PCR was performed using the StepOne™ Real-Time PCR System (Thermo Fisher Scientific). The $2^{-\Delta\Delta Ct}$ method relative expression changes were calculated, and the selected reference group was referenced as 1. GAPDH was used as a reference standard. The PCR primers are listed in Table 1.

Western blot analysis

We used 10% SDS-PAGE (Aspen Biotechnology, Wuhan, China) to separate proteins from cells and mice hearts. After transferred onto a nitrocellulose membrane, the proteins were blocked with skim milk (Aspen Biotechnology) in 10% Tris-buffered saline with Tween (TBST; Aspen Biotechnology) for 2 h. The membranes were incubated at 4 °C with different primary antibodies overnight, then incubated with secondary antibodies for 2 h at room temperature. The experiments were conducted in triplicate and GAPDH was used as the loading control. The information of primary and secondary antibodies used is displayed in Table 2.

Statistical analysis

All analyses were performed using SPSS 23.0 (SPSS Inc., Chicago, IL, USA) and Prism 9.1.2 (GraphPad Software Inc, San Diego, CA, USA). Unpaired *t*-test was used to compare the difference between two groups and One-way ANOVA was used for the difference among groups. Data are shown as means ± standard deviation (SD), each experiment was repeated at least thrice. $P < 0.05$ was considered statistically significant.

Results

TGF-β contributes to the injury and EndMT of HCMECs

As shown in Figure 1A, TGF-β reduced cell viability in a time-dependent manner. After 24 h of treatment with TGF-β, the cell viability of the TGF-β group did not significantly differ from that of the control group ($P > 0.05$). However, compared with the control group, there were significant differences in cell viability after 48, 72, and 96 h of treatment ($P < 0.05$). Therefore, follow-up experiments were performed using a 48-h incubation period with TGF-β. Figure 1B–D shows that the expression levels of α-SMA and FSP-1 were elevated, while that of CD31 was decreased after 48 h of TGF-β treatment ($P < 0.05$). These results suggested that the TGF-β-induced injury and EndMT model in HCMECs was successfully established during treatment with TGF-β for 48 h.

LINC00961 inhibits apoptosis induced by TGF-β in HCMECs

We observed that LINC00961 was significantly expressed in stable overexpression cell lines and remarkably reduced in knockdown cell lines. Additionally, PCR revealed that LINC00961 expression in the TGF-β group was significantly reduced compared with that in the control group ($P < 0.05$) (Figure 2A–B). As shown in Figure 2C–D, LINC00961 overexpression recovered cell viability that had been negatively affected by TGF-β, whereas LINC00961 knockdown exacerbated cell viability that had been negatively affected by TGF-β. Flow cytometric analysis was used to determine the rate of apoptosis, and it revealed that LINC00961 expression could reduce TGF-β-induced apoptosis. However, TGF-β-mediated apoptosis was further facilitated by LINC00961 knockdown (Figure 2E–2F). The mRNA transcription levels of the anti-apoptotic proteins Bcl2 and CyclinD1 were both decreased by TGF-β but recovered when LINC00961 was overexpressed and further reduced when LINC00961 was knocked down, while the mRNA transcription level of proapoptotic protein BAX was reversed (Figure 2G–2H). In addition, western blotting

was used to determine the changes in protein levels. We found the same change tendency of protein level as that of the mRNA transcription level (Figure 2I–2K). Our results indicate that TGF-β-mediated apoptosis was inhibited by LINC00961.

LINC00961 suppresses the TGF-β-induced EndMT

As shown in Figure 3, immunofluorescence staining, qRT-PCR, and western blotting results indicated that VE-cadherin and CD31 expression was significantly downregulated ($P < 0.05$). In contrast, FSP1 and α-SMA expression levels were significantly upregulated ($P < 0.05$) in the TGF-β group relative to those in the control group. VE-cadherin and CD31 expression levels were significantly upregulated ($P < 0.05$), while FSP-1 and α-SMA expression levels were significantly downregulated ($P < 0.05$) in the TGF-β + LV-LINC00961 group compared with those in the TGF-β group. VE-cadherin and CD31 expression levels were significantly downregulated ($P < 0.05$), whereas FSP-1 and α-SMA expression levels were significantly upregulated ($P < 0.05$) in the TGF-β + LV-sh LINC00961 group than those in the TGF-β group. These results suggest that TGF-β-induced EndMT could be suppressed by LINC00961.

LINC00961 attenuates EndMT through the TGF-β - SMAD2/3 signaling pathway

Immunofluorescence staining indicated that CD31 expression was significantly downregulated ($P < 0.05$), whereas α-SMA expression level was significantly upregulated ($P < 0.05$) in the + TGF-β group compared with that in the control group (Figure 4A). Furthermore, CD31 and α-SMA expression was significantly upregulated ($P < 0.05$) in the TGF-β+LV-sh LINC00961 group relative to that in the TGF-β group. However, the expression level was reversed when the TGF-β+LV-sh LINC00961 group was treated with SB431542. As shown in Figure 4B–4I, qRT-PCR results showed that CD31 mRNA transcription levels were significantly downregulated ($P < 0.05$), while SMAD2, SMAD3, SNAIL, SLUG, Pi3k, AKT, and α-SMA mRNA transcription levels were significantly upregulated ($P < 0.05$) in the TGF-β group compared with those in the control group. Furthermore, qRT-PCR results indicated that CD31 mRNA, SMAD2, SMAD3, SNAIL, SLUG, Pi3k, AKT, and α-SMA mRNA transcription levels were significantly upregulated ($P < 0.05$) in the TGF-β+LV-sh LINC00961 group relative to those in the TGF-β group. However, the mRNA transcription level was reversed when the TGF-β+LV-sh LINC00961 group was treated with SB431542. Western blotting results indicated that CD31 protein levels were significantly downregulated ($P < 0.05$), whereas TGF-β1, P-SMAD2/3, SNAIL, SLUG, P-Pi3k, P-AKT, and α-SMA protein levels were significantly upregulated ($P < 0.05$) in the TGF-β group compared with those in the control group (Figure 4J–4R). Meanwhile, CD31, TGF-β1, P-SMAD2/3, SNAIL, SLUG, P-Pi3k, P-AKT, and α-SMA protein levels were significantly upregulated ($P < 0.05$) in the TGF-β+LV-sh LINC00961 group relative to those in the TGF-β group. However, the protein levels were reversed when the TGF-β+LV-sh LINC00961 group was treated with SB431542. Based on these results, we can conclude that LINC00961 attenuates TGF-β-induced EndMT, and the potential mechanism of action for LINC00961 involves TGF-β-SMAD2/3-SNAIL/SLUG signaling pathway suppression, while also involving the TGF-β-PI3K-AKT signaling pathway.

MI contributes to cardiac function deterioration and myocardial fibrosis in LINC00961$^{-/-}$ mice

Figure 5A–5B shows that LINC00961 knockout mice were successfully produced. Representative echocardiograms are shown in Figure 6A. As shown in Figure 6B, we found that the LVEDD and LVESD volumes were both significantly increased in the LINC00961$^{-/-}$ + MI group compared with those in the WT + MI group ($P < 0.05$), while the LVFS and LVEF volumes were both significantly decreased in the LINC00961$^{-/-}$ + MI group than those in the WT + MI group ($P < 0.05$). However, the LVEDD, LVESD, LVFS, and LVEF did not significantly differ between the LINC00961$^{-/-}$ + Sham and the WT + Sham groups ($P > 0.05$). Representative images of H&E and Masson's trichrome staining are shown in Figure 6C–D. As shown in Figure 6E, we observed that the collagen volume fraction (CVF) was significantly increased in the LINC00961$^{-/-}$ + MI group compared with that of the WT + MI group ($P < 0.05$), while it did not significantly differ between the LINC00961$^{-/-}$ + Sham and WT + Sham groups ($P > 0.05$). Immunohistochemical analysis (Figure 6 F–I) revealed that CD31 and VE-cadherin expression was significantly downregulated in the LINC00961$^{-/-}$ + MI group relative to the WT + MI group ($P < 0.05$), while the α-SMA and FSP-1 volumes were both significantly increased in the LINC00961$^{-/-}$ + MI group than those in the WT + MI group ($P < 0.05$). However, CD31, VE-cadherin, α-SMA, and FSP-1 did not significantly differ between the LINC00961$^{-/-}$ + Sham and the WT + Sham groups ($P > 0.05$). Based on these results, MI contributes to cardiac function deterioration and myocardial fibrosis in LINC00961$^{-/-}$ mice; furthermore, LINC00961 preserved cardiac function and attenuated myocardial fibrosis following MI.

SB-431542 preserves cardiac function and attenuates MI-induced myocardial fibrosis

Representative echocardiograms are shown in Figure 7A. As shown in Figure 7B, we found that the LVEDD and LVESD volumes were both significantly decreased in the LINC00961$^{-/-}$ + MI + SB group vs. the LINC00961$^{-/-}$ + MI group ($P < 0.05$), WT + MI + SB group vs. WT + MI group ($P < 0.05$. In addition, the LVFS and LVEF volume were both significantly increased in the LINC00961$^{-/-}$ + MI + SB group vs. the LINC00961$^{-/-}$ + MI group ($P < 0.05$), and WT + MI + SB group vs. WT + MI group ($P < 0.05$). Representative images of H&E and Masson's trichrome staining are shown in Figure 7C–D. We observed that the collagen volume fraction (CVF) was significantly decreased in the LINC00961$^{-/-}$ + MI + SB group vs. the LINC00961$^{-/-}$ + MI group ($P < 0.05$) and WT + MI + SB group vs. WT + MI group ($P < 0.05$; Figure 7E). From the representative immunohistochemical analysis images (Figure 7F–I), it can be seen that CD31 and VE-cadherin expression was significantly upregulated in both the LINC00961$^{-/-}$ + MI + SB group vs. the LINC00961$^{-/-}$ + MI group ($P < 0.05$) and WT + MI + SB group vs WT + MI group ($P < 0.05$), and both α-SMA and FSP-1 volumes were significantly reduced in the LINC00961$^{-/-}$ + MI + SB group vs. the LINC00961$^{-/-}$ + MI group ($P < 0.05$) and WT + MI + SB group vs WT + MI group ($P < 0.05$). Based on these results, SB-431542 was concluded to preserve cardiac function and attenuate MI-induced myocardial fibrosis.

LINC00961 preserves cardiac function and attenuates MI-induced myocardial fibrosis through the TGF-β-SMAD2/3 signaling pathway

As shown in Figure 8A–8H, we demonstrated that SMAD2, SMAD3, SNAIL, SLUG, α-SMA, PI3K, and AKT mRNA expression was significantly upregulated ($P < 0.05$), and CD31 mRNA expression was significantly downregulated ($P < 0.05$) in the LINC00961$^{-/-}$ + MI group compared with those in the LINC00961$^{-/-}$ + Sham group. Furthermore, SMAD2, SMAD3, SNAIL, SLUG, α-SMA, PI3K, AKT, and CD31 mRNA expression patterns were reversed ($P < 0.05$) in the LINC00961$^{-/-}$ + MI + SB group. On the other hand, the p-PI3K/PI3K and p-AKT/AKT ratios, and TGF-β1, P-SMAD2/3, SNAIL, SLUG, and α-SMA protein levels were significantly upregulated ($P < 0.05$), whereas CD31 protein level was significantly downregulated ($P < 0.05$) in the LINC00961$^{-/-}$ + MI group relative to the LINC00961$^{-/-}$ + Sham group. A reversed pattern was observed for the p-PI3K/PI3K and p-AKT/AKT ratios and protein levels (TGF-β1, P-SMAD2/3, SNAIL, SLUG, and α-SMA, CD31) in the LINC00961$^{-/-}$ + MI + SB group ($P < 0.05$). Based on these results, we can conclude that LINC00961 preserves cardiac function and attenuates MI-induced myocardial fibrosis, and the potential mechanism of action for LINC00961 involves suppression of the TGF-β-SMAD2/3-SNAIL/SLUG signaling pathway, as well as the TGF-β-PI3K-AKT signaling pathway. Figure 9 is a schematic showing the connections among the aforementioned proteins and their roles.

Discussion

The efficacy of LINC00961 in inhibiting tumor growth, invasion, and metastasis and regulating endothelial cell function has been extensively documented [37-39]. Considering the association of LINC00961 with the initiation and progression of cardiovascular diseases [40-42], our study aimed to identify the effect of LINC00961 on EndMT and its influence on the TGF-β-SMAD2/3 signaling pathway *in vitro* and *in vivo*, as well as the progression of cardiovascular diseases.

EndMT has been previously identified as an important process in the development of cardiac fibrosis.[43] During EndMT, resident endothelial cells acquire a mesenchymal phenotype characterized by acquiring mesenchymal markers (FSP-1and α-SMA), acquisition of migratory and invasive properties, loss of endothelial markers (VE-cadherin and CD31), loss of cell–cell junctions, and delamination from organized cell layers.[44] Here, we present evidence that cells exposed to TGF-β exhibited increased Bax, caspase, α-SMA, and FSP-1 expression and decreased BCL-2, Cyclin D1, CD31, and VE-cadherin expression. However, LINC00961 treatment reversed these changes. These findings demonstrate that LINC00961 is an effective therapeutic strategy for decreasing endothelial cell injury and EndMT caused by TGF-β.

To explore the underlying mechanism of action of LINC00961, SB-431542, a TGF-β inhibitor, was used. TGF-β increased the levels of TGF-β1, P-SMAD2/3, SNAIL, SLUG, P-Pi3k, P-AKT, and α-SMA proteins, while reducing the level of CD31 protein. When the TGF-β signaling pathway was blocked using SB-431542, the effect of LINC00961 knockdown on TGF-β1, P-SMAD2/3, SNAIL, SLUG, P-Pi3k, P-AKT, and α-SMA protein levels was diminished. These results provide substantial evidence for the original assumption that LINC00961 attenuates TGF-β-induced EndMT and myocardial fibrosis following MI by inhibiting the TGF-β-SMAD2/3-SNAIL/SLUG signaling pathway, consistent with previous studies. Furthermore, recent studies have suggested that LINC00961 downregulation promotes proliferation and

inhibits apoptosis of vascular smooth muscle cells by sponging miR-367 in patients with coronary heart disease[45]. Moreover, the LINC00961/SPAAR locus contributes to cardiac endothelial cell and fibroblast function, hypoxic response, growth and development, and basal cardiovascular function in adulthood[42]. Due to the association of the TGF-β-SMAD2/3-SNAIL/SLUG signaling pathway with EndMT, LINC00961 has been considered a potential therapeutic target to attenuate EndMT and myocardial fibrosis. Here, we demonstrated for the first time that LINC00961 has a protective effect against endothelial cell injury and can attenuate EndMT and myocardial fibrosis following MI by inhibiting the TGF-β-SMAD2/3-SNAIL/SLUG signaling pathway.

Nevertheless, some researchers confirmed that STAT1-mediated LINC00961 aggravated MI via the PI3K/AKT/ GSK3β pathway[40], and we have confirmed that P-PI3K and P-AKT proteins upregulated when LINC00961 knockdown or knockout; hence further studies should elucidate this divergence. The experimental data presented here were obtained using a single endothelial cell line (HCMEC); therefore, to enhance the validity of our results, further studies should investigate the effects of LINC00961 in other endothelial cell lines and myocardial cells. Furthermore, only some molecules involved in the TGF-β-SMAD2/3 and TGF-β-PI3K-AKT signaling pathways, myocardial fibrosis, and EndMT were examined. Further studies should elucidate the relationship between TGF-β-SMAD2/3 and TGF-β-PI3K-AKT signaling pathways.

In conclusion, we revealed that LINC00961 attenuates endothelial injuries and EndMT *in vitro* and myocardial fibrosis following MI *in vivo* by inhibiting the TGF-β-SMAD2/3-SNAIL/SLUG signaling pathway. These findings suggest that it is highly likely that LINC00961 may exert a protective effect against cardiovascular disease.

Declarations

Acknowledgments

We would like to thank Editage (www.editage.cn) for English language editing.

Sources of Funding

This study was supported by Qingdao Outstanding Health Professional Development Fund and the National Natural Science Foundation of China (91180374).

Disclosures

The authors have declared that no competing interest exists.

References

1. Talman V, Ruskoaho H. Cardiac fibrosis in myocardial infarction-from repair and remodeling to regeneration. *Cell and tissue research*. 2016;365:563-581

2. Vaskova E, Ikeda G, Tada Y, Wahlquist C, Mercola M, Yang PC. Sacubitril/valsartan improves cardiac function and decreases myocardial fibrosis via downregulation of exosomal mir-181a in a rodent chronic myocardial infarction model. *Journal of the American Heart Association*. 2020;9:e015640

3. Liu W, Sun J, Guo Y, Liu N, Ding X, Zhang X, Chi J, Kang N, Liu Y, Yin X. Calhex231 ameliorates myocardial fibrosis post myocardial infarction in rats through the autophagy-nlrp3 inflammasome pathway in macrophages. *J Cell Mol Med*. 2020;24:13440-13453

4. Peet C, Ivetic A, Bromage DI, Shah AM. Cardiac monocytes and macrophages after myocardial infarction. *Cardiovasc Res*. 2020;116:1101-1112

5. Moe GW, Marín-García J. Role of cell death in the progression of heart failure. *Heart failure reviews*. 2016;21:157-167

6. Li F, Guo S, Wang C, Huang X, Wang H, Tan X, Cai Q, Wu J, Zhang Y, Chen X, Lin W, Zhang B. Yiqihuoxue decoction protects against post-myocardial infarction injury via activation of cardiomyocytes pgc-1α expression. *BMC complementary and alternative medicine*. 2018;18:253

7. Pei HF, Hou JN, Wei FP, Xue Q, Zhang F, Peng CF, Yang Y, Tian Y, Feng J, Du J, He L, Li XC, Gao EH, Li D, Yang YJ. Melatonin attenuates postmyocardial infarction injury via increasing tom70 expression. *Journal of pineal research*. 2017;62

8. Chi YC, Shi CL, Zhou M, Liu Y, Zhang G, Hou SA. Selective cyclooxygenase-2 inhibitor ns-398 attenuates myocardial fibrosis in mice after myocardial infarction via snail signaling pathway. *Eur Rev Med Pharmacol Sci*. 2017;21:5805-5812

9. Shibamoto M, Higo T, Naito AT, Nakagawa A, Sumida T, Okada K, Sakai T, Kuramoto Y, Yamaguchi T, Ito M, Masumura Y, Higo S, Lee JK, Hikoso S, Komuro I, Sakata Y. Activation of DNA damage response and cellular senescence in cardiac fibroblasts limit cardiac fibrosis after myocardial infarction. *International heart journal*. 2019;60:944-957

10. Matsumoto A, Pasut A, Matsumoto M, Yamashita R, Fung J, Monteleone E, Saghatelian A, Nakayama KI, Clohessy JG, Pandolfi PP. Mtorc1 and muscle regeneration are regulated by the linc00961-encoded spar polypeptide. *Nature*. 2017;541:228-232

11. Tajbakhsh S. Lncrna-encoded polypeptide spar(s) with mtorc1 to regulate skeletal muscle regeneration. *Cell Stem Cell*. 2017;20:428-430

12. Jiang B, Liu J, Zhang YH, Shen D, Liu S, Lin F, Su J, Lin QF, Yan S, Li Y, Mao WD, Liu ZL. Long noncoding rna linc00961 inhibits cell invasion and metastasis in human non-small cell lung cancer. *Biomed Pharmacother*. 2018;97:1311-1318

13. Mu X, Mou KH, Ge R, Han D, Zhou Y, Wang LJ. Linc00961 inhibits the proliferation and invasion of skin melanoma by targeting the mir-367/pten axis. *Int J Oncol*. 2019;55:708-720

14. Wu H, Dai Y, Zhang D, Zhang X, He Z, Xie X, Cai C. Linc00961 inhibits the migration and invasion of colon cancer cells by sponging mir-223-3p and targeting sox11. *Cancer Med*. 2020;9:2514-2523

15. Zhang L, Shao L, Hu Y. Long noncoding rna linc00961 inhibited cell proliferation and invasion through regulating the wnt/β-catenin signaling pathway in tongue squamous cell carcinoma. *J Cell Biochem*. 2019;120:12429-12435

16. Spencer HL, Sanders R, Boulberdaa M, Meloni M, Cochrane A, Spiroski AM, Mountford J, Emanueli C, Caporali A, Brittan M, Rodor J, Baker AH. The linc00961 transcript and its encoded micropeptide spaar regulate endothelial cell function. *Cardiovasc Res*. 2020

17. Liu S, He Y, Shi J, Liu L, Ma H, He L, Guo Y. Stat1-avtiviated linc00961 regulates myocardial infarction by the pi3k/akt/gsk3β signaling pathway. *J Cell Biochem*. 2019;120:13226-13236

18. Markwald RR, Fitzharris TP, Smith WN. Sturctural analysis of endocardial cytodifferentiation. *Developmental biology*. 1975;42:160-180

19. Bischoff J. Endothelial-to-mesenchymal transition. *Circ Res*. 2019;124:1163-1165

20. Potenta S, Zeisberg E, Kalluri R. The role of endothelial-to-mesenchymal transition in cancer progression. *British journal of cancer*. 2008;99:1375-1379

21. Liu X, Mujahid H, Rong B, Lu QH, Zhang W, Li P, Li N, Liang ES, Wang Q, Tang DQ, Li NL, Ji XP, Chen YG, Zhao YX, Zhang MX. Irisin inhibits high glucose-induced endothelial-to-mesenchymal transition and exerts a dose-dependent bidirectional effect on diabetic cardiomyopathy. *J Cell Mol Med*. 2018;22:808-822

22. Feng B, Cao Y, Chen S, Chu X, Chu Y, Chakrabarti S. Mir-200b mediates endothelial-to-mesenchymal transition in diabetic cardiomyopathy. *Diabetes*. 2016;65:768-779

23. Yin Y, Zhang Q, Zhao Q, Ding G, Wei C, Chang L, Li H, Bei H, Wang H, Liang J, Jia Z. Tongxinluo attenuates myocardiac fibrosis after acute myocardial infarction in rats via inhibition of endothelial-to-mesenchymal transition. *BioMed research international*. 2019;2019:6595437

24. Zheng X, Peng M, Li Y, Wang X, Lu W, Wang X, Shan Y, Li R, Gao L, Qiu C. Cathelicidin-related antimicrobial peptide protects against cardiac fibrosis in diabetic mice heart by regulating endothelial-mesenchymal transition. *Int J Biol Sci*. 2019;15:2393-2407

25. Zou J, Liu Y, Li B, Zheng Z, Ke X, Hao Y, Li X, Li X, Liu F, Zhang Z. Autophagy attenuates endothelial-to-mesenchymal transition by promoting snail degradation in human cardiac microvascular endothelial cells. *Bioscience reports*. 2017;37

26. Liu Y, Zou J, Li B, Wang Y, Wang D, Hao Y, Ke X, Li X. Runx3 modulates hypoxia-induced endothelial-to-mesenchymal transition of human cardiac microvascular endothelial cells. *Int J Mol Med*.

2017;40:65-74

27. Hu J, Zheng Z, Li X, Li B, Lai X, Li N, Lei S. Metformin attenuates hypoxia-induced endothelial cell injury by activating the amp-activated protein kinase pathway. *J Cardiovasc Pharmacol*. 2021;77:862-874

28. Derynck R, Budi EH. Specificity, versatility, and control of tgf-β family signaling. *Sci Signal*. 2019;12

29. Medici D, Potenta S, Kalluri R. Transforming growth factor-β2 promotes snail-mediated endothelial-mesenchymal transition through convergence of smad-dependent and smad-independent signalling. *The Biochemical journal*. 2011;437:515-520

30. Miyazono K, Katsuno Y, Koinuma D, Ehata S, Morikawa M. Intracellular and extracellular tgf-β signaling in cancer: Some recent topics. *Front Med*. 2018;12:387-411

31. Morikawa M, Derynck R, Miyazono K. Tgf-β and the tgf-β family: Context-dependent roles in cell and tissue physiology. *Cold Spring Harb Perspect Biol*. 2016;8

32. Song S, Zhang R, Cao W, Fang G, Yu Y, Wan Y, Wang C, Li Y, Wang Q. Foxm1 is a critical driver of tgf-β-induced endmt in endothelial cells through smad2/3 and binds to the snail promoter. *J Cell Physiol*. 2019;234:9052-9064

33. Ghosh AK, Nagpal V, Covington JW, Michaels MA, Vaughan DE. Molecular basis of cardiac endothelial-to-mesenchymal transition (endmt): Differential expression of microrna s during endmt. *Cell Signal*. 2012;24:1031-1036

34. Zhou F, Wang M, Luo T, Qu J, Chen WR. Photo-activated chemo-immunotherapy for metastatic cancer using a synergistic graphene nanosystem. *Biomaterials*. 2021;265:120421

35. Zhang M, Weng H, Zheng J. Nad(+) repletion inhibits the endothelial-to-mesenchymal transition induced by tgf-β in endothelial cells through improving mitochondrial unfolded protein response. *Int J Biochem Cell Biol*. 2019;117:105635

36. Hjelmeland MD, Hjelmeland AB, Sathornsumetee S, Reese ED, Herbstreith MH, Laping NJ, Friedman HS, Bigner DD, Wang XF, Rich JN. Sb-431542, a small molecule transforming growth factor-beta-receptor antagonist, inhibits human glioma cell line proliferation and motility. *Mol Cancer Ther*. 2004;3:737-745

37. Pan LN, Sun YR. Linc00961 suppresses cell proliferation and induces cell apoptosis in oral squamous cell carcinoma. *Eur Rev Med Pharmacol Sci*. 2019;23:3358-3365

38. Chen D, Zhu M, Su H, Chen J, Xu X, Cao C. Linc00961 restrains cancer progression via modulating epithelial-mesenchymal transition in renal cell carcinoma. *J Cell Physiol*. 2019;234:7257-7265

39. Zhang L, Shao L, Hu Y. Long noncoding rna linc00961 inhibited cell proliferation and invasion through regulating the wnt/beta-catenin signaling pathway in tongue squamous cell carcinoma. *J Cell Biochem*. 2019;120:12429-12435

40. Liu S, He Y, Shi J, Liu L, Ma H, He L, Guo Y. Stat1-avtiviated linc00961 regulates myocardial infarction by the pi3k/akt/gsk3beta signaling pathway. *J Cell Biochem*. 2019;120:13226-13236

41. Wu CT, Liu S, Tang M. Downregulation of linc00961 contributes to promote proliferation and inhibit apoptosis of vascular smooth muscle cell by sponging mir-367 in patients with coronary heart disease. *Eur Rev Med Pharmacol Sci*. 2019;23:8540-8550

42. Spiroski AM, Sanders R, Meloni M, McCracken IR, Thomson A, Brittan M, Gray GA, Baker AH. The influence of the linc00961/spaar locus loss on murine development, myocardial dynamics, and cardiac response to myocardial infarction. *International journal of molecular sciences*. 2021;22

43. Zeisberg EM, Tarnavski O, Zeisberg M, Dorfman AL, McMullen JR, Gustafsson E, Chandraker A, Yuan X, Pu WT, Roberts AB, Neilson EG, Sayegh MH, Izumo S, Kalluri R. Endothelial-to-mesenchymal transition contributes to cardiac fibrosis. *Nature medicine*. 2007;13:952-961

44. Piera-Velazquez S, Li Z, Jimenez SA. Role of endothelial-mesenchymal transition (endmt) in the pathogenesis of fibrotic disorders. *The American journal of pathology*. 2011;179:1074-1080

45. C.-T. WU SL, M. TANG. Downregulation of linc00961 contributes to promote proliferation and inhibit apoptosis of vascular smooth muscle cell by sponging mir-367 in patients with coronary heart disease. *Eur Rev Med Pharmacol Sci*. 2019:8540-8550

Tables

Table 1 The primarys used in the qRT-PCR assay

Gene name		Primer sequence
CD31	forward	5’-ACCAAGATAGCCTCAAAGTCGG-3’
	reverse	5’-TAAGAAATCCTGGGCTGGGAG-3’
VE-Cadherin	forward	5’-AAGGACATAACACCACGAAACG-3’
	reverse	5’-GAGATGACCACGGGTAGGAAG-3’
α-SMA	forward	5’-CTATGCCTCTGGACGCACAAC-3’
	reverse	5’-CCCATCAGGCAACTCGTAACTC-3’
FSP-1	forward	5’-GGTGTCCACCTTCCACAAGTAC-3’
	reverse	5’-TCCTGGGCTGCTTATCTGG-3’
CyclinD1	forward	5’-TCCTACTTCAAATGTGTGCAGAAG-3’
	reverse	5’-CATCTTAGAGGCCACGAACATG-3’
Bcl-2	forward	5’-AGGATTGTGGCCTTCTTTGAG-3’
	reverse	5’-AGCCAGGAGAAATCAAACAGAG-3’
Bax	forward	5’-TCTGAGCAGATCATGAAGACAGG-3’
	reverse	5’-ATCCTCTGCAGCTCCATGTTAC-3’
AKT	forward	5’-TTCTATGGCGCTGAGATTGTGT-3’
	reverse	5’-GCCGTAGTCATTGTCCTCCAG-3’
SMAD2	forward	5’-AGTGAGGAGCCAGGGGAGA -3’
	reverse	5’-TTACAGCAAAGGTTGAGGAAGG -3’
LINC00961	forward	5’-ATGGAAACGGCAGTGATTGG-3’
	reverse	5’-GGCGTCACATGAAGGTCCAG-3’
SMAD3	forward	5’-TCACCGACCCCTCCAATTC -3
	reverse	5’-GCCGCACGCCTCTTCC -3
PI3K	forward	5’-GTCCTATTGTCGTGCATGTGG-3
	reverse	5’-TGGGTTCTCCCAATTCAACC-3
GAPDH	forward	5’-CATCATCCCTGCCTCTACTGG-3’
	reverse	5’-GTGGGTGTCGCTGTTGAAGTC-3’
SNAIL	forward	5’-AATCCAGAGTTTACCTTCCAGC -3’
	reverse	5’-GAAGTAGAGGAGAAGGACGAAG -3’

SLUG	forward	5’-CTGTGACAAGGAATATGTGTGAGC -3’
	reverse	5’-CTAATGTGTCCTTGAAGCAACC -3’

Table 2 The imformation aboat primary and secondary antibodies

Primary antibodies	Species	Venders	Catelogue number	Dilution
GAPDH	Rabbit	Abcam (Cambridge, MA)	ab37168	1:10000
TGF-β	Rabbit	Abcam (Cambridge, MA)	ab215715	1:1000
P-PI3k	Rabbit	Abcam (Cambridge, MA)	ab182651	1:500
PI3k	Rabbit	CST (Danvers, MA)	#4292	1:3000
P-AKT	Rabbit	CST (Danvers, MA)	#4060	1:1000
AKT	Rabbit	CST (Danvers, MA)	#9272	1:2000
SPARR	Rabbit	CST (Danvers, MA)	#25823	1:1000
P-SMAD2/3	Rabbit	Santa Cruz (Dallas, TX)	Sc-11769	1:500
SNAIL	Rabbit	Abcam (Cambridge, MA)	ab216347	1:1000
CD31	Mouse	Santa Cruz (Dallas, TX)	Sc-376764	1:500
VE-Cadherin	Rabbit	Therm (Waltham, MA)	36-1900	1:500
α-SMA	Rabbit	ProteinTech (Chicago, IL)	14395-1-AP	1:5000
FSP-1	Rabbit	ProteinTech (Chicago, IL)	20886-1-AP	1:1000
CyclinD1	Rabbit	CST (Danvers, MA)	#55506	1:1000
Bcl-2	Rabbit	Abcam (Cambridge, MA)	Ab59348	1:1000
Bax	Rabbit	CST (Danvers, MA)	#2772	1:2000
SLUG	Rabbit	Abcam (Cambridge, MA)	Ab27568	1:1000
Cleaved caspase3	Rabbit	Abcam (Cambridge, MA)	Ab49822	1:500
Secondary antibodies		**Venders**	**Catelogue number**	**Dilution**
HRP-goat anti rabit		ASPEN (Wuhan, China)	AS1107	1:10000
HRP-goat anti Mouse		ASPEN (Wuhan, China)	AS1106	1:10000

Figures

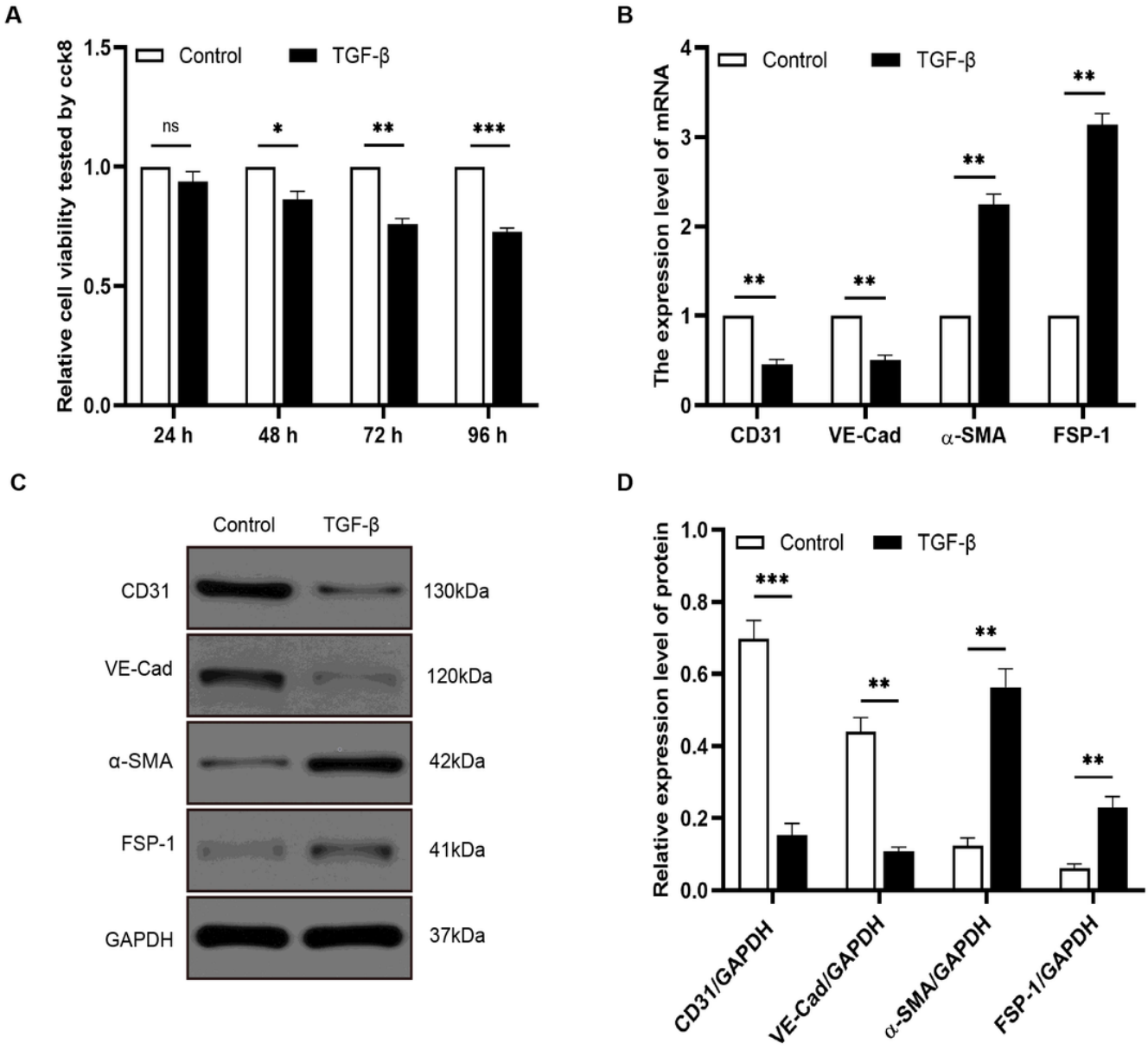

Figure 1

TGF-β contributes to the injury and EndMT of HCMECs Notes: (A) Cell viability was measured using a CCK8 assay when HCMECs were exposed to TGF-β (10 ng/mL; Peprotech Inc, Rocky Hill, NJ, USA) for 24, 48, 72, and 96 h. (B) RT-qPCR was conducted to test the expression levels of CD31, VE-Cad, α-SMA, and FSP-1 mRNA. (C–D) Western blotting was conducted to test the expression levels of CD31, VE-Cad, α-SMA, and FSP-1 proteins. Each experiment was conducted in triplicate; ns $P > 0.05$, *$P < 0.05$, **$P < 0.01$, and ***$P < 0.001$. n = 5 per group. Abbreviations: EndMT, endothelial-mesenchymal transition; HCMEC, human cardiac microvascular endothelial cell; h, hour; CCK8, cell counting kit 8.

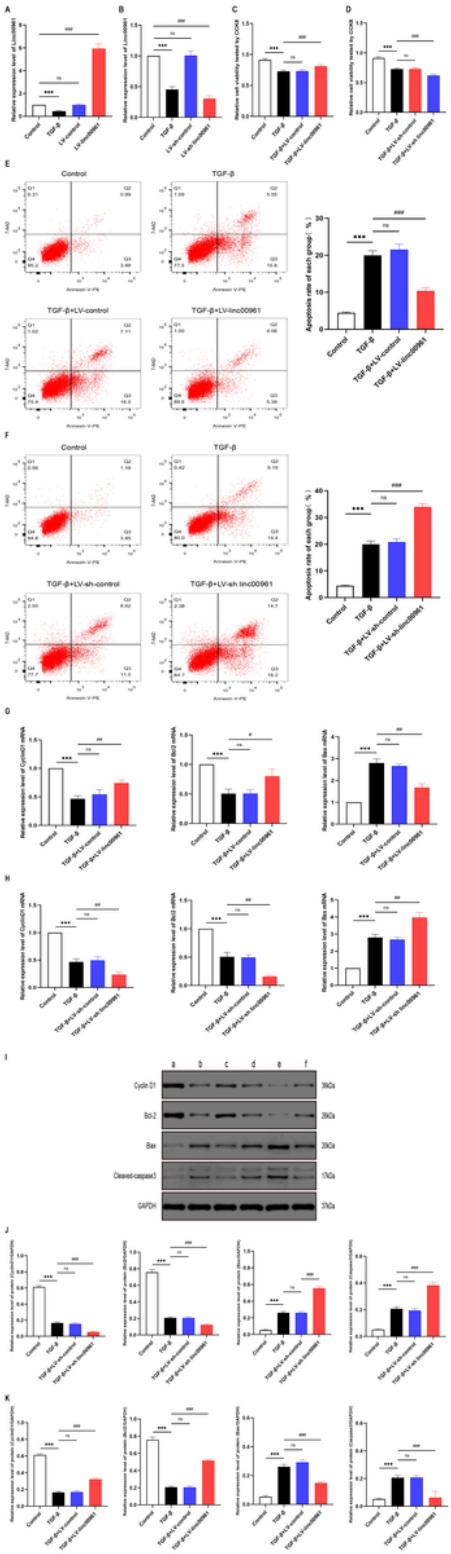

Figure 2

LINC00961 inhibits TGF-β-induced apoptosis in HCMECs Notes: (A–B) RT-qPCR was conducted to test the expression level of LINC00961. (C–D) Cell viability was measured using the CCK8 assay. (E–F) Flow cytometry analysis was performed to evaluate the cell apoptosis rate. (G–H) The expression levels of apoptosis-related mRNA were determined by RT-qPCR. (I–J) The expression levels of apoptosis-related

proteins were determined by western blotting. Each experiment was conducted in triplicate, ns P >0.05, *P < 0.05, #P < 0.05, **P < 0.01, ##P < 0.01, ***P < 0.001, and ###P < 0.001. n=5 per group.

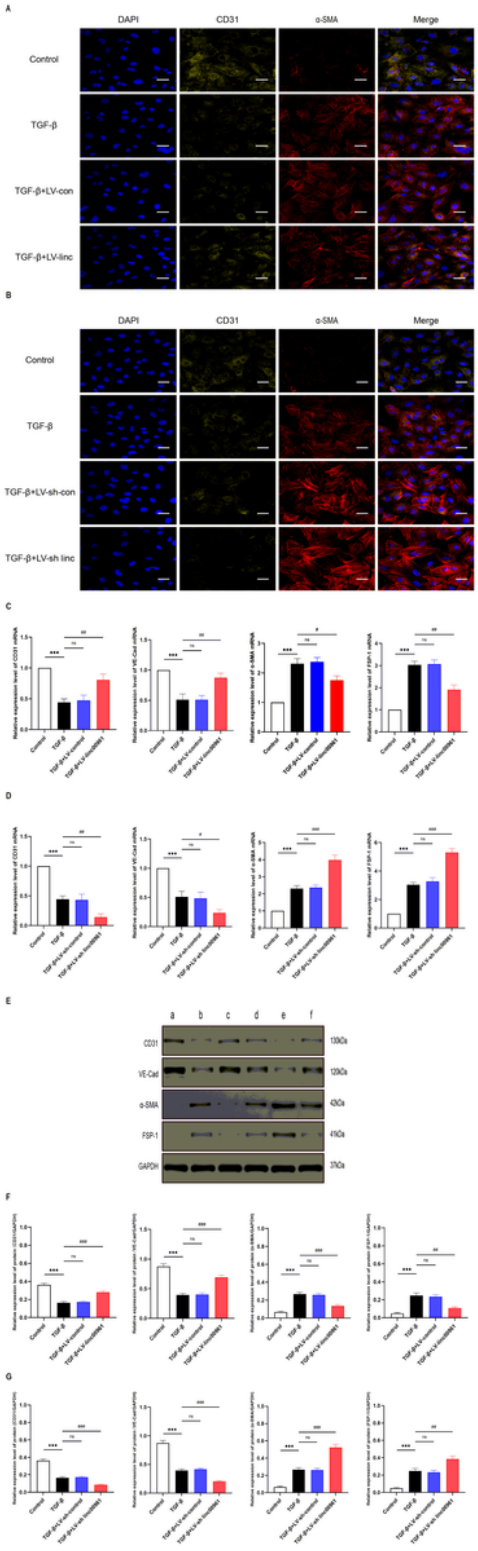

Figure 3

LINC00961 suppresses TGF-β-induced EndMT (A-B) Immunofluorescence staining was used to identify CD31+/α-SMA+ double-positive cells. CD31 (green), α-SMA (red), Scale bars: 50 μm. (C–D) The expression levels of EndMT-related mRNA were determined by RT-qPCR. (E–G) The expression levels of

EndMT-related proteins were determined by western blotting. Each experiment was conducted in triplicate, ns P >0.05, *P < 0.05, #P < 0.05, **P < 0.01, ##P < 0.01, ***P < 0.001, and ###P < 0.001. n=5 per group. Abbreviations: α-SMA, alpha-smooth muscle actin; FSP-1, fibroblast specific protein 1; VE-Cad, VE-cadherin.

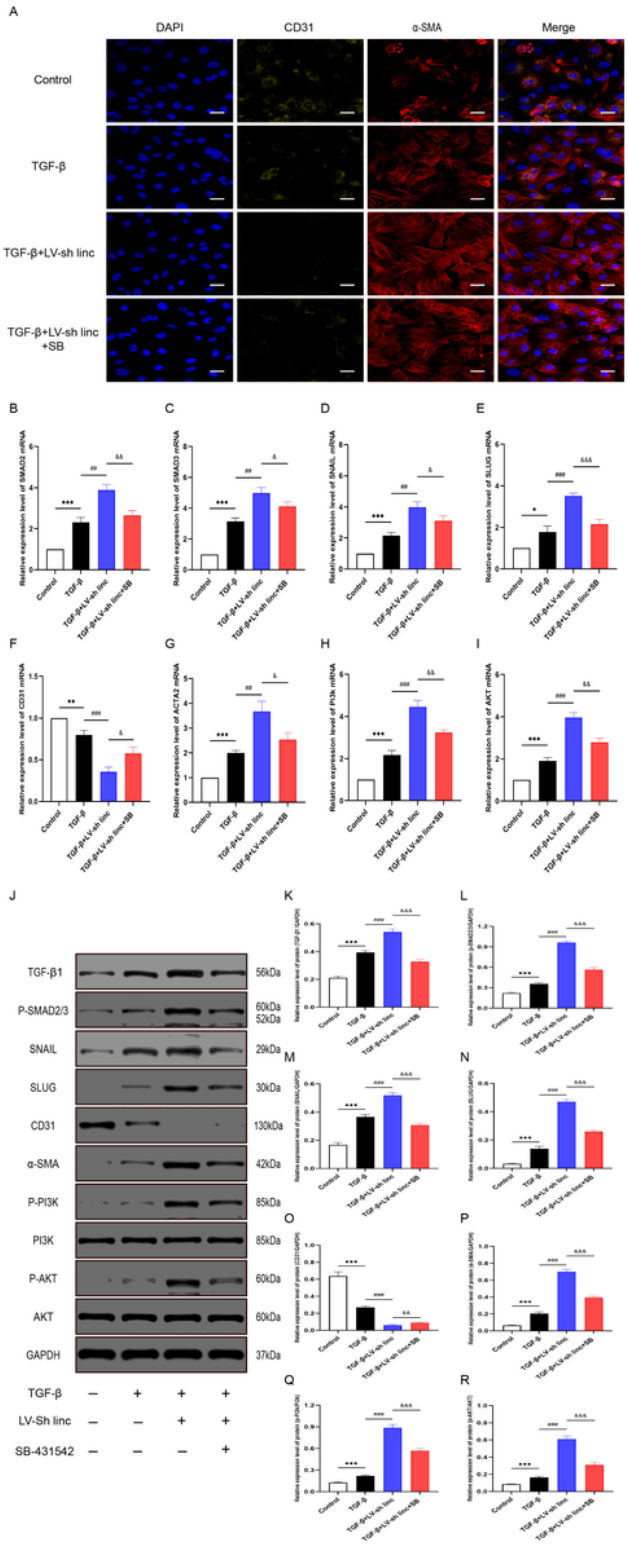

Figure 4

LINC00961 attenuates EndMT through the TGF-β-SMAD2/3 signaling pathway Notes: (A) Immunofluorescence staining was used to identify CD31+/α-SMA+ double-positive cells. CD31 (green), α-SMA (red), Scale bars: 50 μm. (B–I) The expression levels of SMAD2, SMAD3, SNAIL, SLUG, CD31, α-SMA, PI3K, and AKT mRNA were determined by RT-qPCR. (J–R) The expression levels of TGF-β1, P-SMAD2/3, SNAIL, SLUG, CD31, α-SMA, P-PI3K, PI3K, P-AKT, and AKT proteins were determined by western blotting. Each experiment was conducted in triplicate, ns P >0.05, *P < 0.05, #P < 0.05, &P < 0.05, **P < 0.01, ##P < 0.01, &&P < 0.01, ***P < 0.001, ###P < 0.001, and &&&P < 0.001. n=5 per group. Abbreviations: SMAD, small mother against decapentaplegic; TGF-β1, transforming growth factor β1; PI3K, phosphatidylinositol-3-kinase; mTOR, mammalian target of rapamycin.

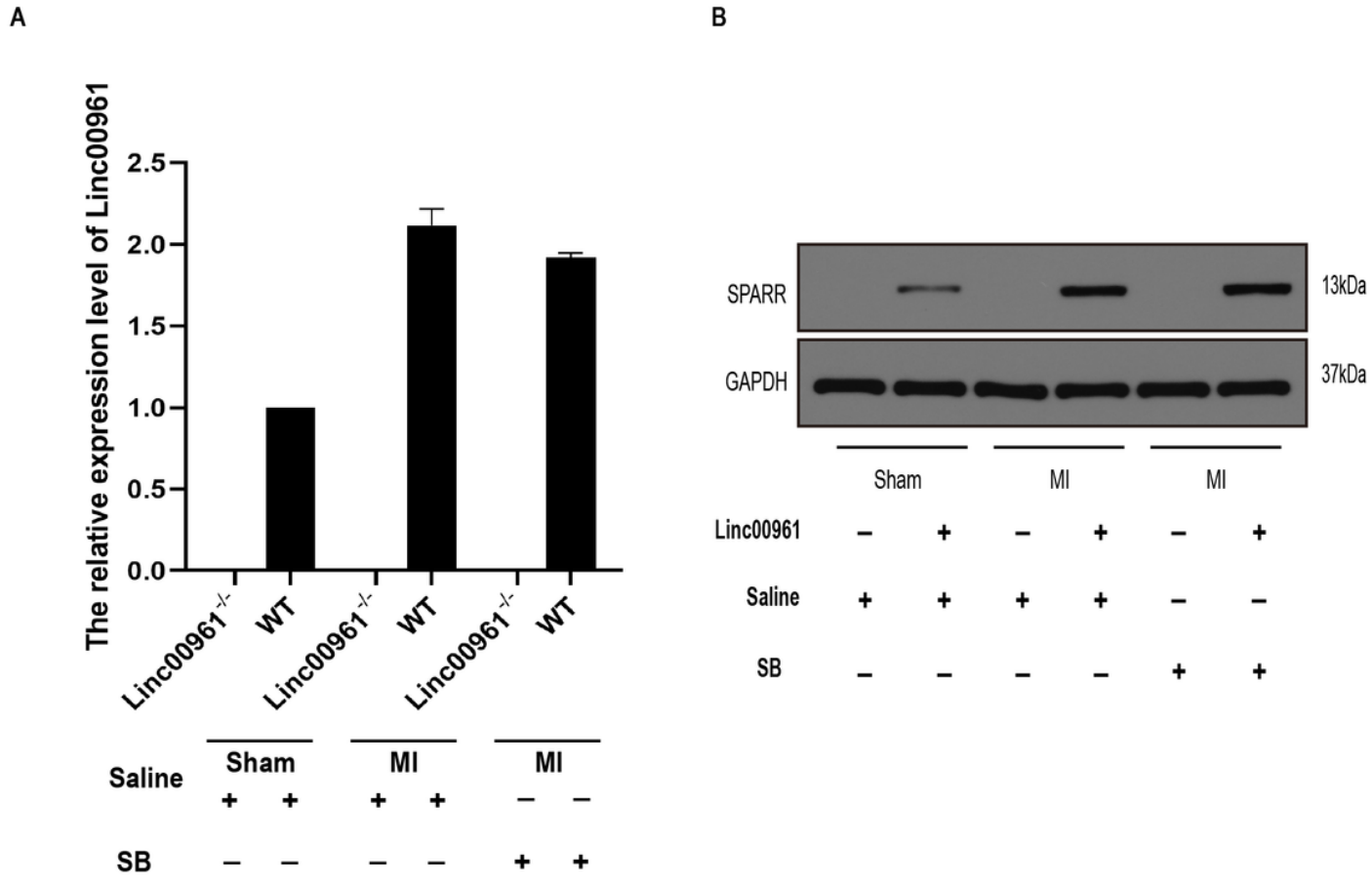

Figure 5

LINC00961-/- mice were successfully produced. Notes: (A) The expression level of LINC00961 was determined by RT-qPCR. (B) The expression level of SPARR protein was determined by western blotting. Abbreviations: WT, wild type; MI, myocardial infarction; SPARR, small regulatory polypeptide of amino acid response.

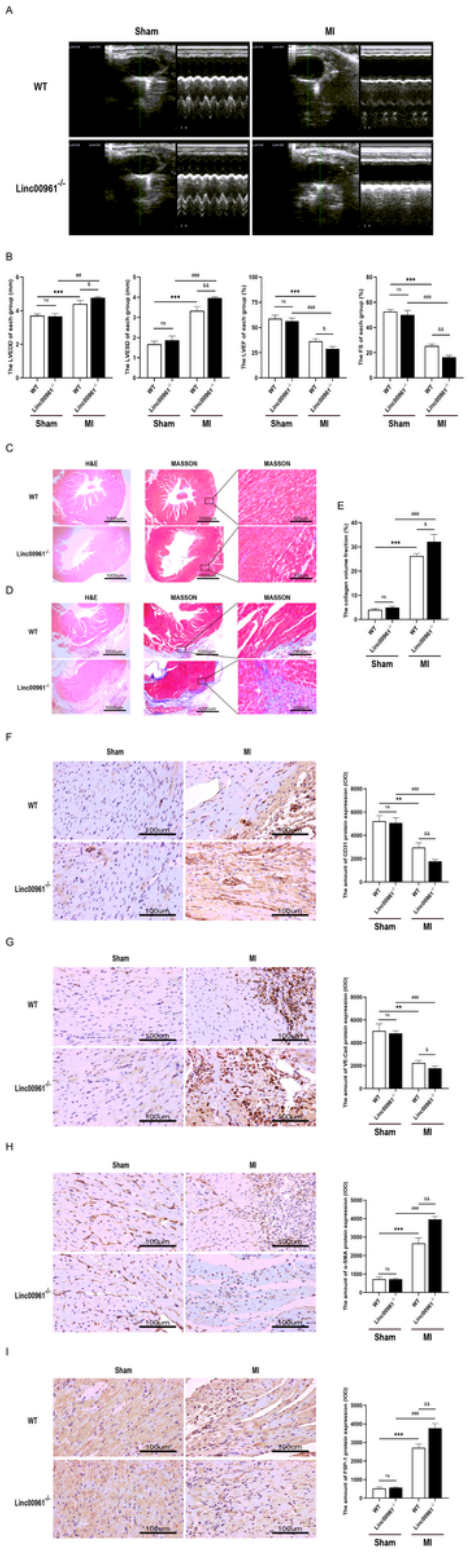

Figure 6

MI contributes to the deterioration of cardiac function and myocardial fibrosis in LINC00961-/- mice (A) Representative transthoracic M-mode echocardiograms from each group. (B) LVEDD, LVESD, LVEF, and LVFS in each group derived from the original echocardiographic records. (C–D) Representative images of Sham and MI groups stained with Masson-Trichrome and hematoxylin-eosin (H&E) after myocardial infarction, Scale bars 100 μm; 1,000 μm. (E) The collagen volume fraction of each group obtained from

Image J. (F–I) Representative CD31, VE-Cad, α-SMA, and FSP-1 immunohistochemical images of each group. Scale bars 100 μm. Each experiment was conducted in triplicate, ns P >0.05, *P < 0.05, #P < 0.05, &P < 0.05, **P < 0.01, ##P < 0.01, &&P < 0.01, ***P < 0.001, ###P < 0.001, and &&&P < 0.001. n=5 per group. Abbreviations: LVEDD, left ventricular end-diastolic diameter; LVESD, left ventricular end-systolic diameter; LVFS, left ventricular fractional shortening; LVEF, left ventricular ejection fraction; IOD, integral optical density.

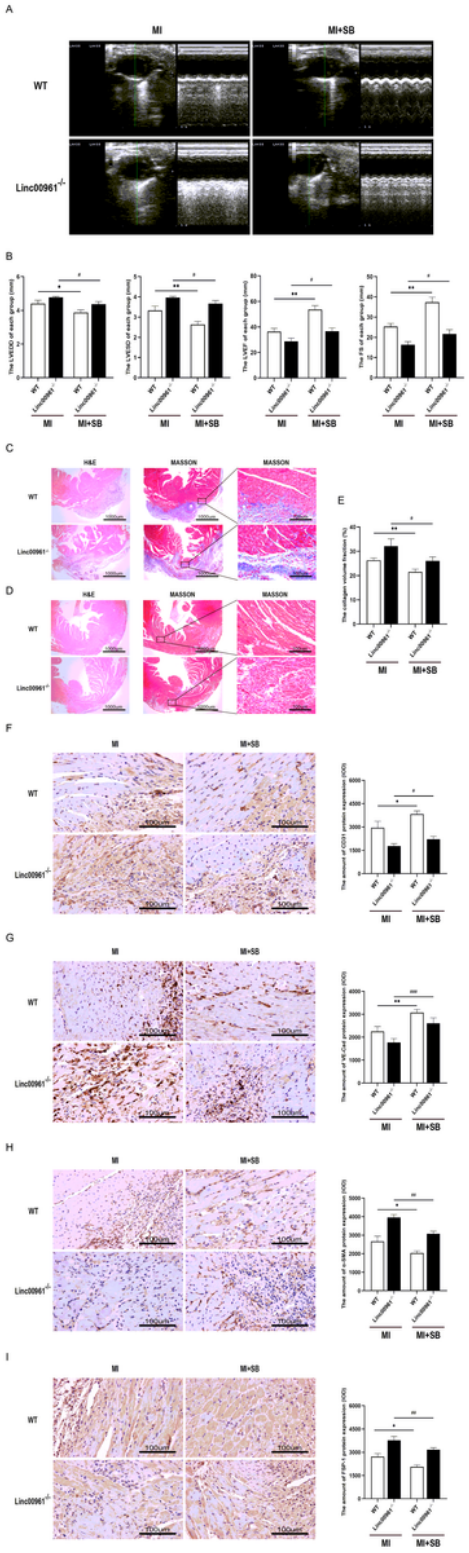

Figure 7

SB-431542 preserves cardiac function and attenuates MI-induced myocardial fibrosis (A) Representative transthoracic M-mode echocardiograms from each group. (B) LVEDD, LVESD, LVEF, and LVFS in each group derived from the original echocardiographic records. (C–D) Representative images of MI and MI + SB groups stained with Masson-Trichrome and hematoxylin-eosin (H&E) after myocardial infarction, Scale bars 100 μm; 1,000 μm. (E) The collagen volume fraction of each group obtained from Image J. (F–I) Representative CD31, VE-Cad, α-SMA, and FSP-1 immunohistochemical images of each group. Scale bars 100 μm. Each experiment was conducted in triplicate, ns $P > 0.05$, *$P < 0.05$, #$P < 0.05$, &$P < 0.05$, **$P < 0.01$, ##$P < 0.01$, &&$P < 0.01$, ***$P < 0.001$, ###$P < 0.001$, and &&&$P < 0.001$. n=5 per group.

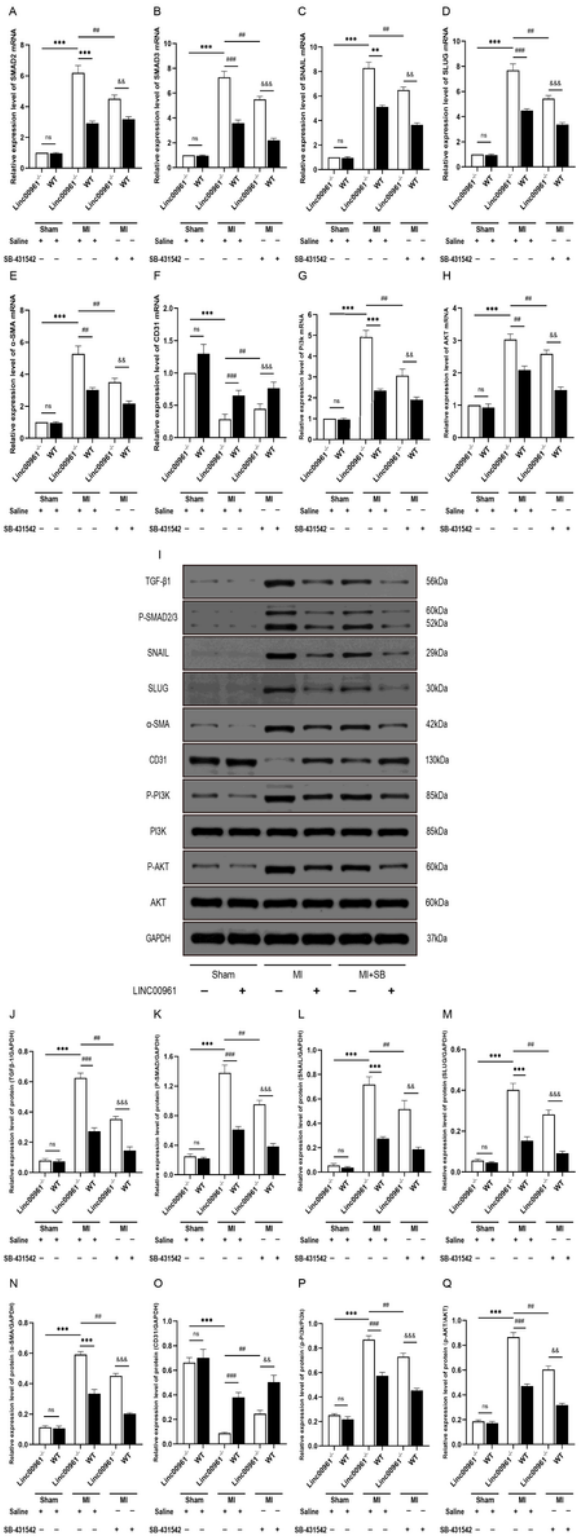

Figure 8

LINC00961 preserves cardiac function and attenuates MI-induced myocardial fibrosis through the TGF-β-SMAD2/3 signaling pathway Notes: (A–H) The expression levels of SMAD2, SMAD3, SNAIL, SLUG, CD31, α-SMA, PI3K, and AKT mRNA were determined by RT-qPCR. (I–Q) The expression levels of TGF-β1, P-SMAD2/3, SNAIL, SLUG, CD31, α-SMA, P-PI3K, PI3K, P-AKT, and AKT proteins were determined by western

blotting. Each experiment was conducted in triplicate, ns P >0.05, *P < 0.05, #P < 0.05, &P < 0.05, **P < 0.01, ##P < 0.01, &&P < 0.01, ***P < 0.001, ###P < 0.001, and &&&P < 0.001. n=5 per group.

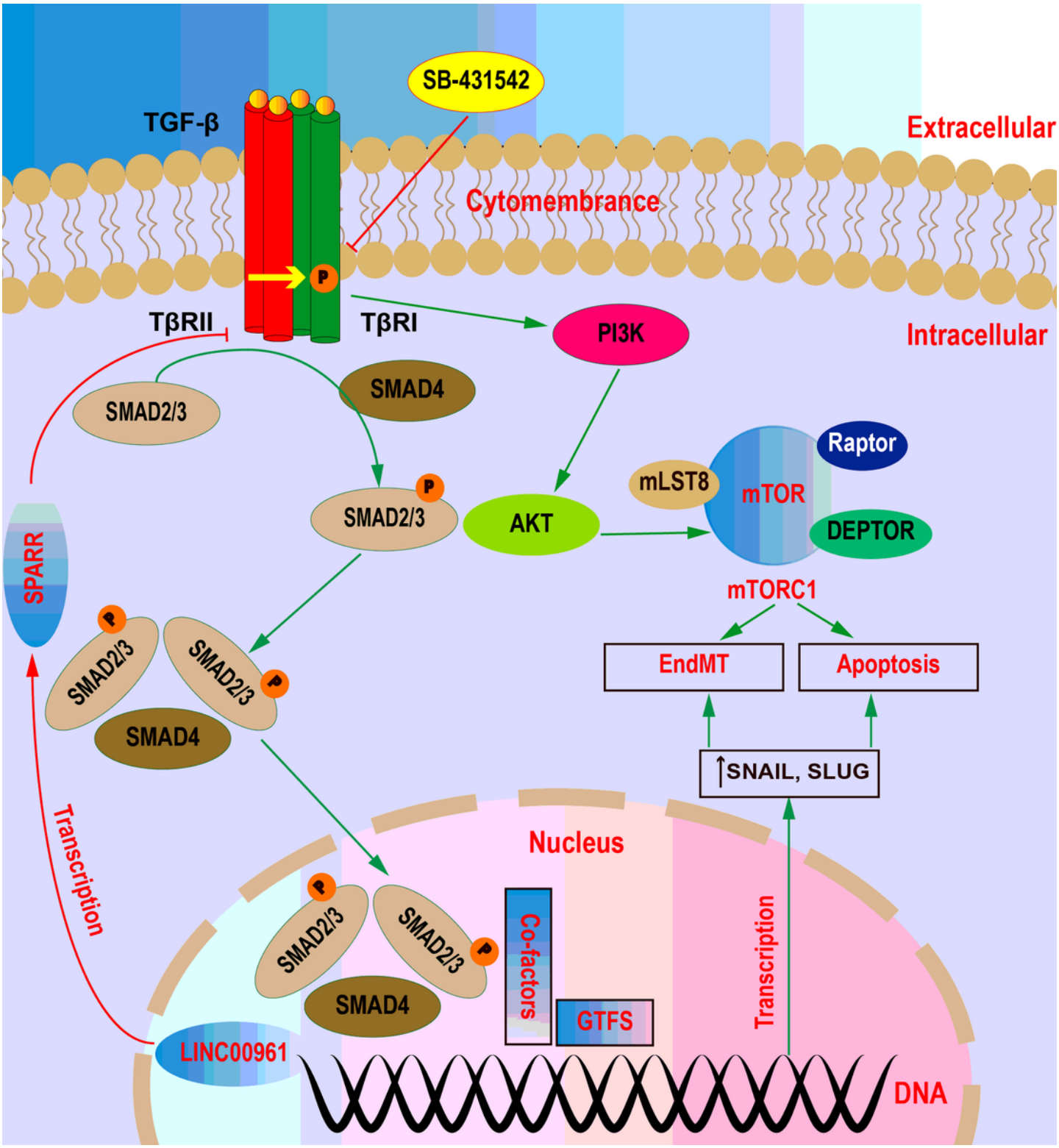

Figure 9

Schematic figure highlighting the connections among identified proteins and their roles. LINC00961 attenuates endothelial injuries and EndMT in vitro, and myocardial fibrosis after myocardial infarction in vivo by inhibiting the TGF-β-SMAD2/3-SNAIL/SLUG signaling pathway, while also involving the TGF-β-

PI3K-AKT signaling pathway. Abbreviations: mTORC1, mTOR complex 1; mLST8, mammalian lethal with Sec13 protein 8; DEPTOR, DEP domain-containing mTOR-interacting protein; Raptor, regulatory-associated protein of mTOR; 4EBP1, eukaryotic translation initiation factor 4E-binding protein 1.